Interaction Notes
Note 470
September, 1988

RESPONSE OF AN OVERHEAD WIRE NEAR A NEMP SIMULATOR

D. Hansen, H. Schaer, D. Koenigstein, H. Hoitink and H. Garbe
Asea Brown Boveri Ltd.
Corporate Research
ABB EMI Control Center
Baden / Switzerland

and

D.V. Giri
Pro-Tech
125 University Avenue
Berkeley, CA 94710

Abstract

The response of an overhead wire illuminated by a simulated nuclear electromagnetic pulse (NEMP) has been experimentally investigated. The wire is 70 m long, 7 mm in diameter and is situated 5 m above the ground. It is located 20 m away from a hybrid type of EMP simulator. The simulator is a resistively loaded elliptical loop structure with its pulse generator located 20 m above the ground. The overhead wire is terminated with various combinations of short circuit, open circuit and characteristic impedance at the two ends and the current response is measured at one end and in the middle. The measured responses are compared with calculated values from available analytical models.

Acknowledgements

The authors wish to thank the Swiss Armament Technology and Procurement Group, Spiez (Swiss Department of Defense) and the Swiss Federal Railway Company for their support and cooperation.

Contents

1. Introduction

Overhead wires and cables carry electric power, communication signals etc., to and from civilian and military facilities located both above the ground and underground. They are integral components of a vast array of facilities, that may be exposed to hostile electromagnetic (EM) environments both manmade and natural. A clear understanding of their interaction with the EM environment is essential for designers concerned with a system's ability to survive the environment. The overhead wire's response to incident EM radiation has been theoretically known [1-3] and in the present work, we have focussed on measuring such responses. The analytical models, for example [1 and 3], have a similar approach in arriving at the response. They treat the bare wire or shielded wire above ground with soil as a return conductor, as a "two-wire" transmission line. The characteristic impedance Z_c and the propagation number γ of this equivalent two-wire line is known [4] in terms of the geometrical parameters and the constitutive parameters of the soil and the cable shield if any. Then the distributed voltage source in the Telegrapher's equations [5] is obtained from the longitudinal component, parallel to the overhead wire, of the electric field. This driving electric field is a sum of incident and ground reflected fields in the absence of the wire or the cable.

The measurements reported in this paper were performed on an overhead wire near the "Mobile" Electromagnetic Pulse Simulator (MEMPS) in Wimmis, Switzerland. MEMPS is operated and maintained by AC Laboratory of the Swiss Department of Defense. MEMPS is an elliptical loop hybrid type of EMP simulator about 20 m high and 60 m wide. The loop structure is resistively loaded and can be excited by a 4 MV pulser, capable of producing approximately 80 kV/m electric field, with a 7 ns rise time directly below the pulser [6]. The overhead wire is however, located at a horizontal distance of 20 m away from the simulator and 5 m above the ground where the horizontal E field is of the order of 25 kV/m. The transmission line formed by the wire with soil as the return conductor is terminated in various combinations of short circuit, open circuit and the characteristic impedance during the experiment. All three components of the incident electric field are computed and they are also measured at a few locations near the transmission line. Coupling of these fields to the transmission line, producing transmission line currents are computed using the transmission line theory of [1] and measured as well. Comparisons are made of the calculated and measured responses.

An additional feature during the experiment was the presence of a 15 m long, 3 m wide and 4.5 m high locomotive of the Swiss Federal Railway Company (SBB) at the center of the 70 m long transmission line. The locomotive was 4.5 m high compared to the 5 m height of the overhead wire and there was no electrical connection between the wire and the locomotive. The presence of the locomotive impacts the wave impedance of the transmission line and also, at least locally disturbs the fields coupling to the line.

This was empirically accounted for, in the coupling computations resulting in better agreement between the theory and experiment.

The various sections of this paper describe the incident field computation and measurement (section 2), the experimental configurations and measurement schemes (section 3), the analytical model (section 4), and comparisons between the theoretical predictions and measurements (section 5).

2. The Incident Field from MEMPS

A generic hybrid type of EMP simulator is shown in figure 1. The dimensions of 20 m height and 60 m width shown are for the Swiss MEMPS. The structure is energized by an EMP pulser at the top as indicated in figure 1. At low frequencies, where the wave lengths are large compared to simulator structure, quasi-static form of the fields is applicable. High frequency (early-time) portion of the wave form reaching the system under test, is radiated from a relatively small source region typically a biconical radiator in the pulser itself. The low frequency (late time) portion of the wave form is associated with the currents and charges distributed over the major dimensions of the simulator structure. The structure is made sparse to avoid high frequency reflections off the structure and it is also impedance loaded to dampen the structure resonances in the intermediate frequency regime.

A rectangular coordinate system (x, y, z), with its origin on the ground directly underneath the pulser is defined, as shown in figure 2. The location of the overhead wire is also indicated. This wire is located at a height of 5 m above the ground, 20 m away from the simulator structure in the z direction. For the purpose of evaluating the wire response, one requires the incident field at the location of the wire, in its absence. Such an incident field is available to us from two sources viz. computed and measured. The computations are based on a method of moments approach [7] for an arbitrary distribution of loaded or unloaded thin wire structures. The computations were made for all three components E_x, E_y, E_z at three locations P_1 (0, 4.5, 20 m), P_2 (-17.5, 4.5, 20 m) and P_3 (-35, 4.5, 20 m).

Recall that z = 20 m is the vertical plane containing the axis of the overhead wire. The three points are located on a horizontal line 0.5 m below and parallel to the wire at one end of the wire, at the center and a point in between. The computations are of course symmetric in the right half of the overhead wire region. A limitation of this computational approach is the use of perfectly conducting ($\sigma_g = \infty$) ground. The electric field distribution along the transmission line was computed under the following assumptions

i) double exponential pulser voltage

$$V_p(t) = V_o \left[e^{-\alpha t} - e^{-\beta t}\right] u(t) \qquad (1)$$

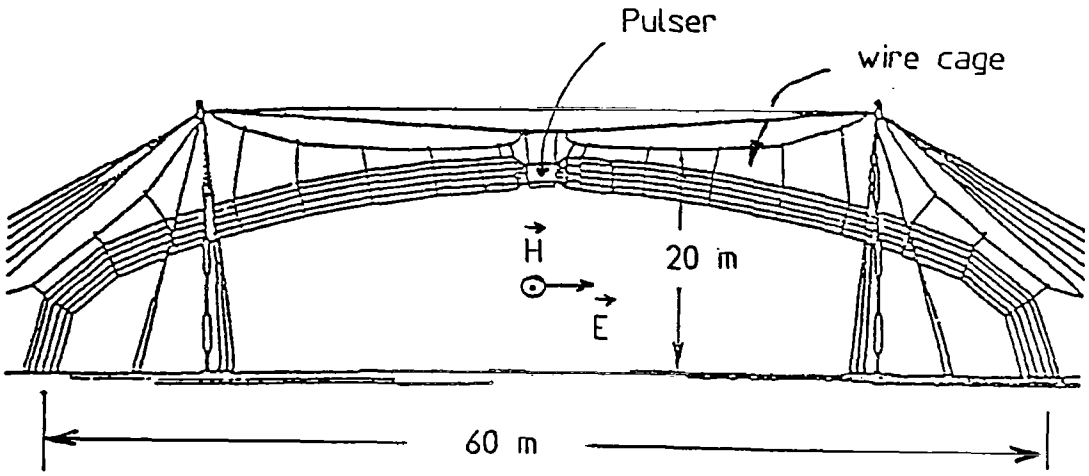

Figure 1. Generic hybrid type of EMP simulator showing the dimensions for MEMPS (not to scale)

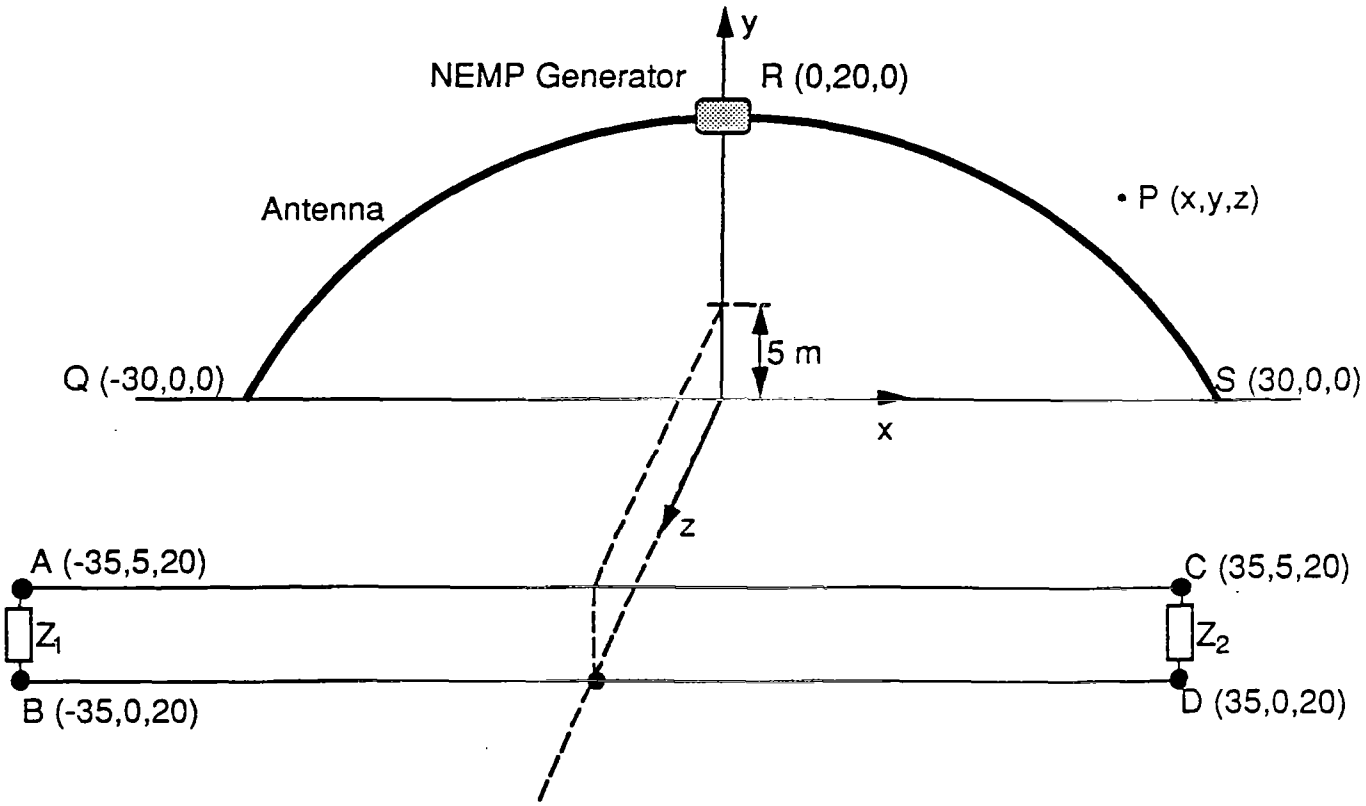

Figure 2. Geometry of the Simulator - Overhead wire in a rectangular coordinate system (the coordinates of various points are in meters)

with V_0 = arbitrary

α = 4×10^6 /s

β = 4.8×10^8 /s

u(t) ≡ unit step function

ii) σ_g ≡ conductivity of ground = ∞

iii) resistive loading of the elliptical structure.

The computed electric field quantities are shown in figure 3.

Recall that the axis of the overhead wire is located in the z = 20 m plane. Figure 3 also indicates the locations of the test points P_1, P_2, and P_3 relative to the wire above the ground in this plane. The top three plots in figure 3 are the axial (parallel to the wire) components of electric field and the bottom three plots are components of electric field parallel to the terminators. It is observed that the principal horizontal component $E_x(x, y, z)$ is fairly uniform along the overhead wire and the vertical component has relatively more variation along the wire. Since the axial electric field is the dominant driver, resulting in distributed voltage sources along the wire, we have focussed our attention on this component of the incident field. From an earlier field mapping effort in and near the simulator facility, the axial electric field (E_x) was available at a few locations near the wire location. These measured axial electric fields are shown plotted in figure 4, once again illustrating the fairly uniform excitation of the overhead wire.

However, an additional feature in our experiment was the presence of an electrical locomotive of the Swiss Federal Railway Company (SBB) at the center of the transmission line. The locomotive's dimensions are length = 15.4 m, height = 3.8 m and width = 2.9 m. Electromagnetically, the locomotive's presence complicates the situation, by impedance loading the transmission line and more importantly by distorting the incident field illuminating the line.

Since the length of the overhead wire is about 4.5 times larger than the length of the locomotive, it is possible to account for its presence by localized corrections to the excitation fields. In other words, the 70 m length of the transmission line may be divided into three sections, with the middle 15 m long section extending over the length of the locomotive and two sections on either side which are 27.5 m long. A localized correction may be applied to the middle section only to account for the presence to the locomotive. Such a correction to the incident field has resulted in better comparisons between the computations and experimental responses, as is seen later in this paper.

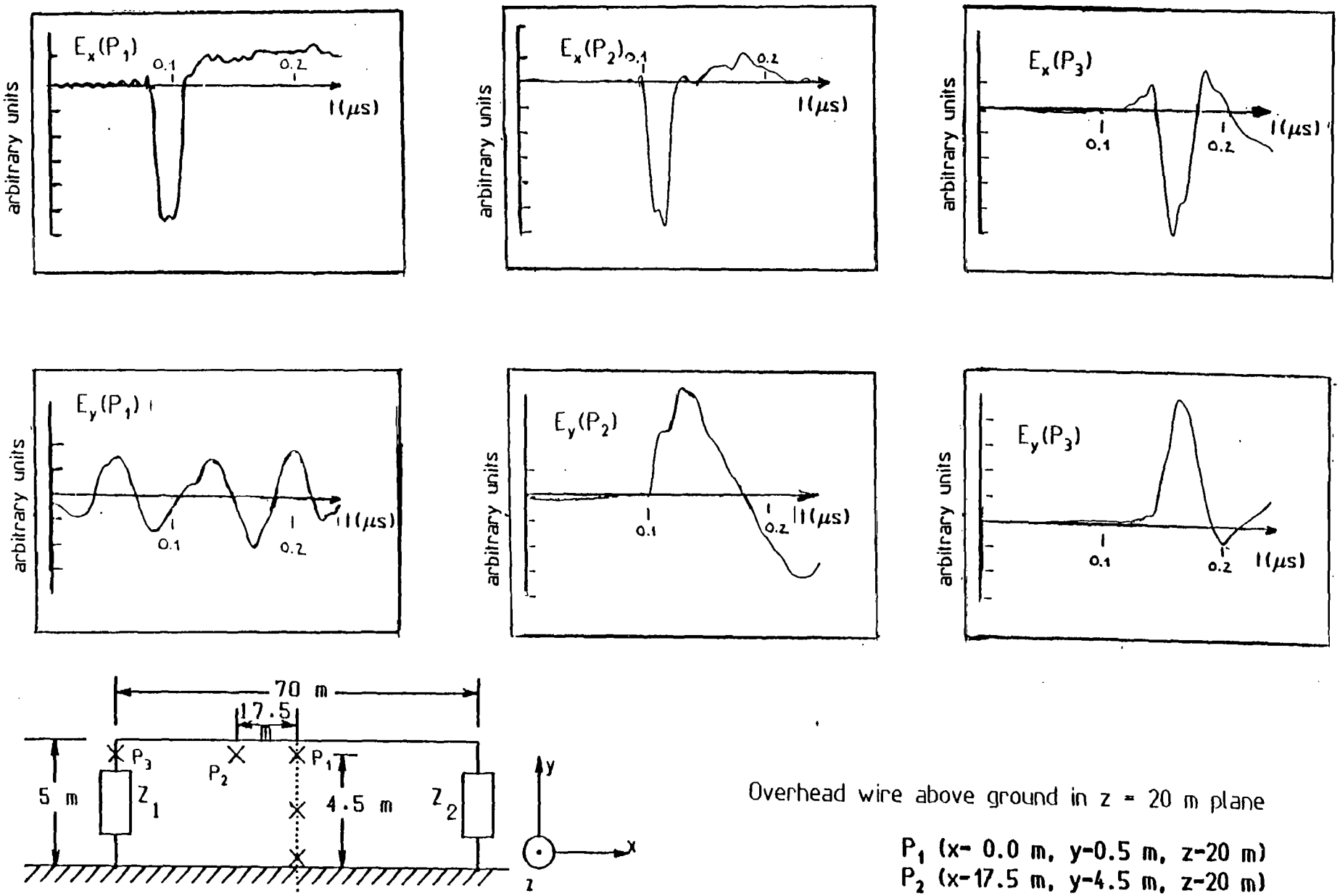

Overhead wire above ground in z = 20 m plane

P_1 (x= 0.0 m, y=0.5 m, z=20 m)
P_2 (x=17.5 m, y=4.5 m, z=20 m)
P_3 (x=35.0 m, y=4.5 m, z=20 m)

Figure 3. Computed components (parallel to wire in x direction and parallel to the terminator in y direction) of the incident electric field.

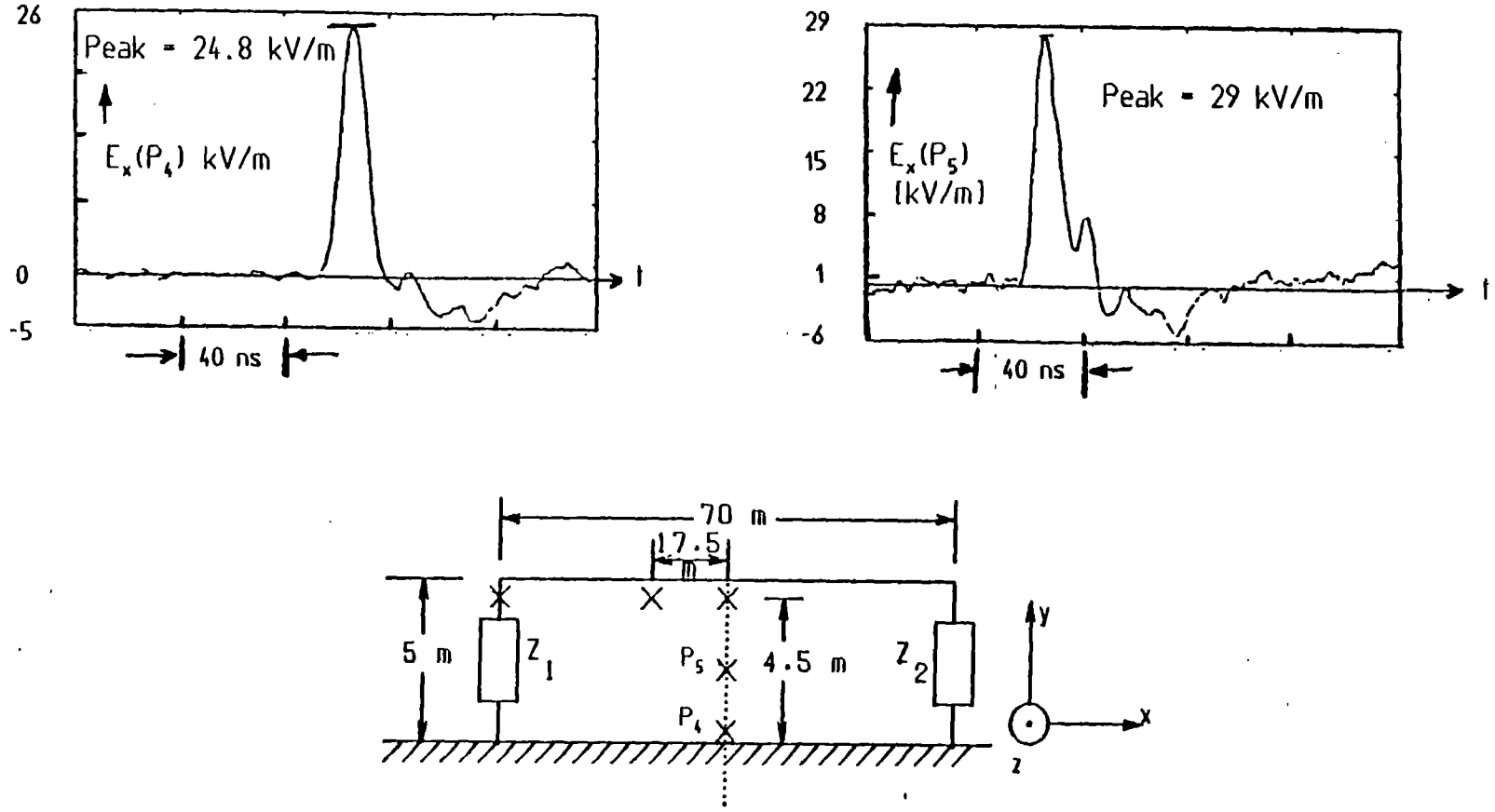

Overhead wire above ground in z = 20 m plane

Figure 4. Measured component of the incident electric fields at test points P_4 and P_5 (available from previous field mapping data at MEMPS).
P_4 (x=0, y=0.5 m, z=22.5 m) and P_5(x=0, y=2.4 m, z=22.5 m)

Returning to the subject of an empirical model for the measured E_x field, it is observed that this field is fairly uniform over the entire length of the wire, in the absence of the wire and the locomotive. Consequently, a double exponential model is proposed and used for the purpose of coupling calculations. So, the uniform excitation field can now be approximately modelled by

$$E_x(t) \simeq E_o \, (e^{-\alpha t} - e^{-\beta t}) \, u(t) \qquad (2)$$

with E_o = 25 kV/m, $\alpha = 4 \times 10^6$/s and $\beta = 4.8 \times 10^8$/s. As described above, this field is incident on the two end sections and a corrected field of the same form is incident in the middle section. The illuminating fields in various sections of the wire illustrated in Figure 5, are empirically given by

$$E_x(x,\ 4.5\ m,\ 20\ m,\ t) \simeq f(x) \, E_o \, (e^{-\alpha t} - e^{-\beta t}) \, u(t) \qquad (3)$$

It is observed that the x dependence is approximated by

$$f(x) = \begin{cases} 1 & x_1 \le x \le x_2 \\ f_2 & x_2 < x < x_3 \\ 1 & x_3 \le x \le x_4 \end{cases}$$

where x_1, x_2, x_3 and x_4 are shown in figure 5. Recall that E_o, α and β are postulated earlier and u(t) is a unit step function of time. The impact of approximating the incident field by the above model is discussed in further detail in section 5. Specifically, we have studied the effect of changing α and β on the eventual current respones. It is however, emphasized that the above model is for the incident field and the total horizontal field is constructed by adding the ground reflections.

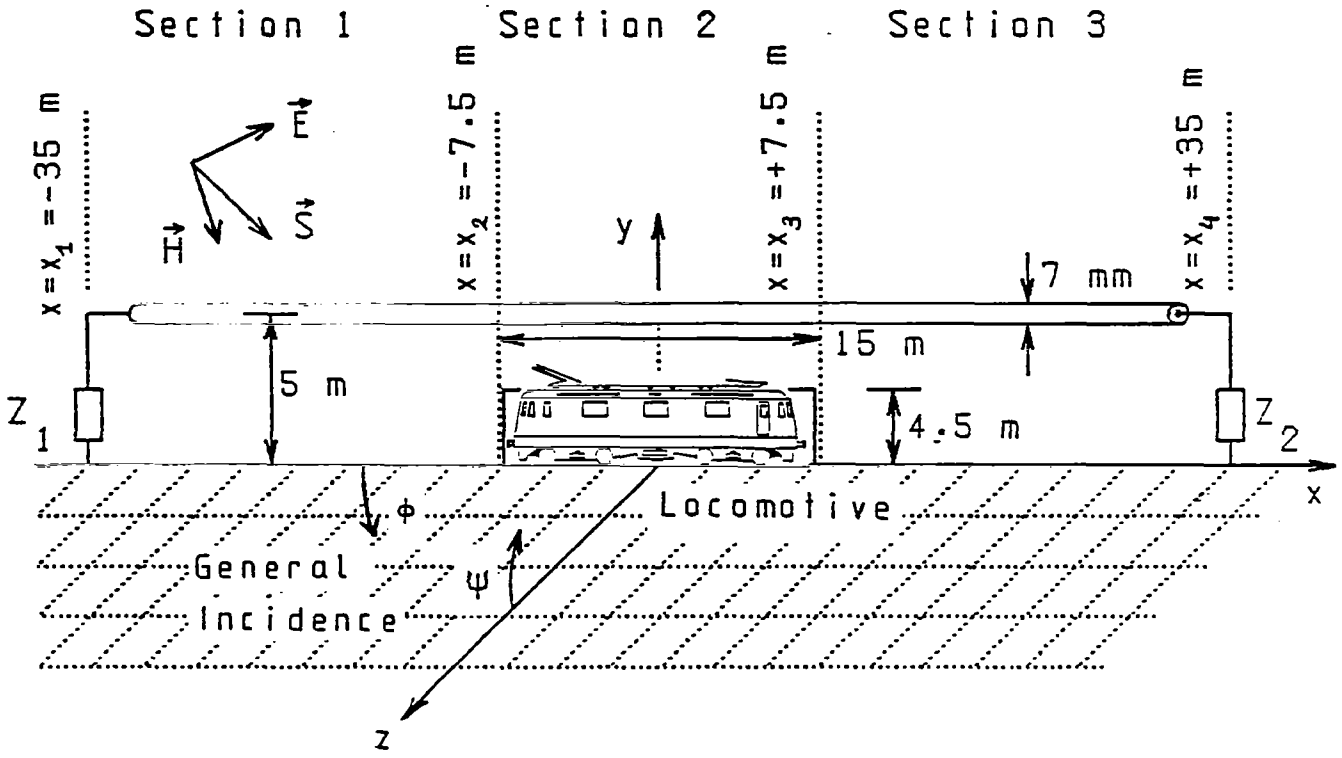

Figure 5. Overhead wire over soil in the z=20 m plane showing the three sections over which the axial E_x field is considered uniform

(Note: The width of the locomotive along the z direction is 3 m, but this information is unused.)

3. The Overhead Wire and Experimental Configurations

Figure 2 has shown the geometry of the simulator and the overhead wire in a rectangular coordinate system and figure 5 shows the location and relevant dimensions of the locomotive present during the experiment. Since the wire and the simulator are fixed in their position, the angle of incidence and polarization of the incident field are fixed. The parameters that can and have been varied in the experiment are:

a) the location along the wire where the current response is measured and

b) the terminating impedances Z_1 and Z_2 on the two ends of the overhead wire. Ten (10) different experimental configurations have been studied and the experimental parameters have been listed in Table 1. The various choices in the experimental parameters are described below.

First of all, the two locations where the induced currents are measured, are $x = -35$ m and $x = -7$ m, corresponding respectively to the end of the line and just above the left edge of the locomotive. The block diagram of the current measurement experiment is shown in figure 6. Secondly, the terminating impedances Z_1 and Z_2 are governed by a requirement for a short circuit, open circuit and the wave impedances. Several combinations are possible and some choices have been made. It is noted however, that the leads connecting the terminators have a combined inductance of .5 μH estimated on the basis of 1 μH/m, and a resistance of 2 mΩ. Consequently, a nominal short circuit becomes $0.002\ \Omega + j\omega(5\mu H)$. Furthermore, the characteristic impedance of the overhead wire above the ground is estimated as a function of frequency, as is seen in detail in the following section.

TABLE 1. Experimental Parameters

Case #	Location x(m) along the wire where the current is measured	Terminating Impedances Z_1 (Ω) (L = 5 μH)	Z_2 (Ω)
1	x = -35 m	600 + jωL	600 + jωL
2	x = -7 m	600 + jωL	600 + jωL
3	x = -35 m	600 + jωL	10^6
4	x = -7 m	600 + jωL	10^6
5	x = -7 m	10^6	600 + jωL
6	x = -35 m	600 + jωL	.002 + jωL
7	x = -7 m	600 + jωL	.002 + jωL
8	x = -7 m	10^6	10^6
9	x = -35 m	.002 + jωL	.002 + jωL
10	x = -7 m	.002 + jωL	.002 + jωL

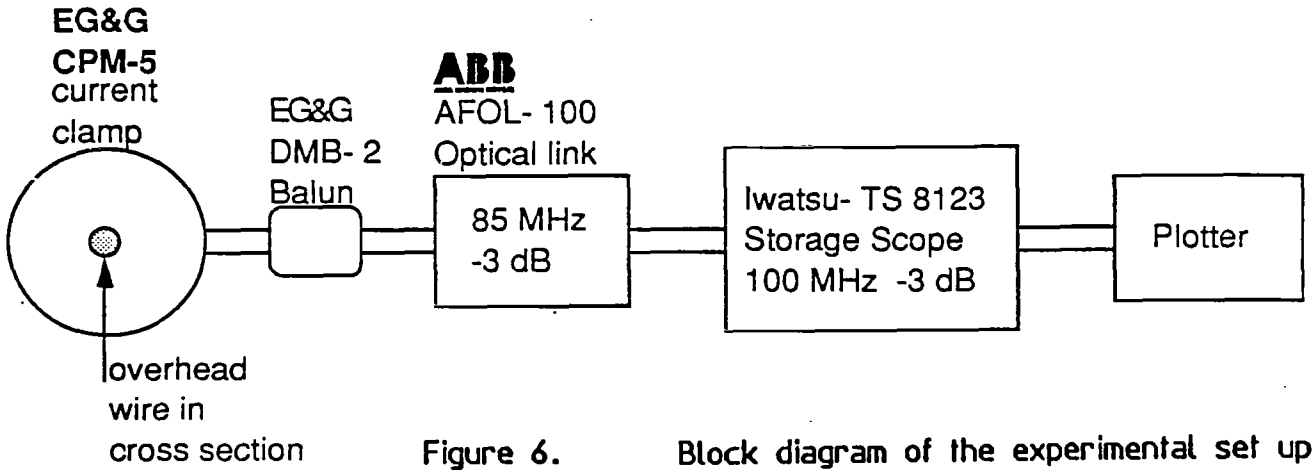

Figure 6. Block diagram of the experimental set up for current measurement.

4. Analytical Model Used for Comparison

For an aerial wire of radius a and height h above the ground, the characteristic impedance $\tilde{Z}_c$ and the propagation factor γ are given by [1],

$$\tilde{Z}_c \simeq \frac{Z_o}{2\pi} \ln\left(\frac{2h}{a}\right) (1 + \Lambda) \tag{5}$$

$$\gamma \simeq \frac{s}{c} (1 + \Lambda) \tag{6}$$

where

Z_o = characteristic impedance of free space = 377 Ω

s = complex frequency = $\Omega + j\omega$, (Ω can be set = 0) ---> $s = j\omega$

ω = $2\pi f \equiv$ radian frequency

c = speed of light = 3×10^8 m/s

and
$$\Lambda = \frac{1}{2 \ln\left(\frac{2h}{a}\right)} \left[\ln\left(\frac{1 + \sqrt{j\omega\tau_h}}{\sqrt{j\omega\tau_h}}\right)\right] \tag{7}$$

where $\tau_h = \mu_o \sigma_g h^2$ and σ_g = soil or ground conductivity.

The above expressions for $\tilde{Z}_c$ and γ are strictly valid when the series impedance $\tilde{Z}_g$ and shunt admittance $\tilde{Y}_g$ of the ground medium are negligible compared with the series inductance ($j\omega L$) and shunt admittance ($j\omega C$) terms of a conventional two-wire line. The expressions for $\tilde{Z}_g$ and $\tilde{Y}_g$ are also available [1] as follows

$$\tilde{Z}_g \simeq \frac{-j\,\gamma_s}{4\,\pi h \sigma_g} \frac{H_o^{(1)}(j\,\gamma_s\,2\,h)}{H_1^{(1)}(j\,\gamma_s\,2\,h)} \tag{8}$$

$$\tilde{Y}_g \simeq \frac{\gamma_s^2}{\tilde{Z}_g} \tag{9}$$

with
$$\gamma_s = \sqrt{j\,\omega\,\mu_o\,(\sigma_g + j\,\omega\,\varepsilon_o\,\varepsilon_r)} \tag{10}$$

We have computed the magnitude of the wave impedance $|\tilde{Z}_c|$ as a function of frequency with and without considering the ground parameters $\tilde{Z}_g$ and $\tilde{Y}_g$, for the case of $\sigma_g = 10^{-2}\Omega^{-1}/m$ and $\sigma_g = \infty$. The results are shown plotted in figure 7. It is seen that above a frequency of about 10 kHz, the two curves are nearly the same. Consequently, in the transmission line response, differences will be observed in computations at very late times if we use the exact or approximate expressions for $\tilde{Z}_c$. Such late time responses are not of present interest. Noting the low frequency behaviour of $|\tilde{Z}_c|$, it is observed that an "average" value of 600 Ω is a reasonable value for termination. Recall that this value of impedance is terminating the overhead wire to the ground. If $\sigma_g = \infty$, the characteristic impedance of the two wire line would then be twice this value. The differential equation of second order for the current along the transmission line for harmonically varying signals [$\exp(j\omega t)$] is

$$\frac{d^2\tilde{I}}{dx^2} - \gamma^2 \tilde{I} = -\tilde{Y}' E_x \tag{11}$$

where $\gamma^2 = \tilde{Z}'\tilde{Y}'$ with $\tilde{Z}'$ and $\tilde{Y}'$ being the impedance and admittance per unit length. The solution to above equation may be written as [1],

$$\tilde{I}(\omega,x) = [\tilde{K}_1 + \tilde{P}(x)]\, e^{-\gamma x} + [\tilde{K}_2 + \tilde{Q}(x)]\, e^{\gamma x} \tag{12}$$

where

$$\tilde{P}(x) = \frac{1}{2\tilde{Z}_c} \int_{x_1}^{x} e^{\gamma v}\, \tilde{E}_x(\omega,v)\, dv \tag{13}$$

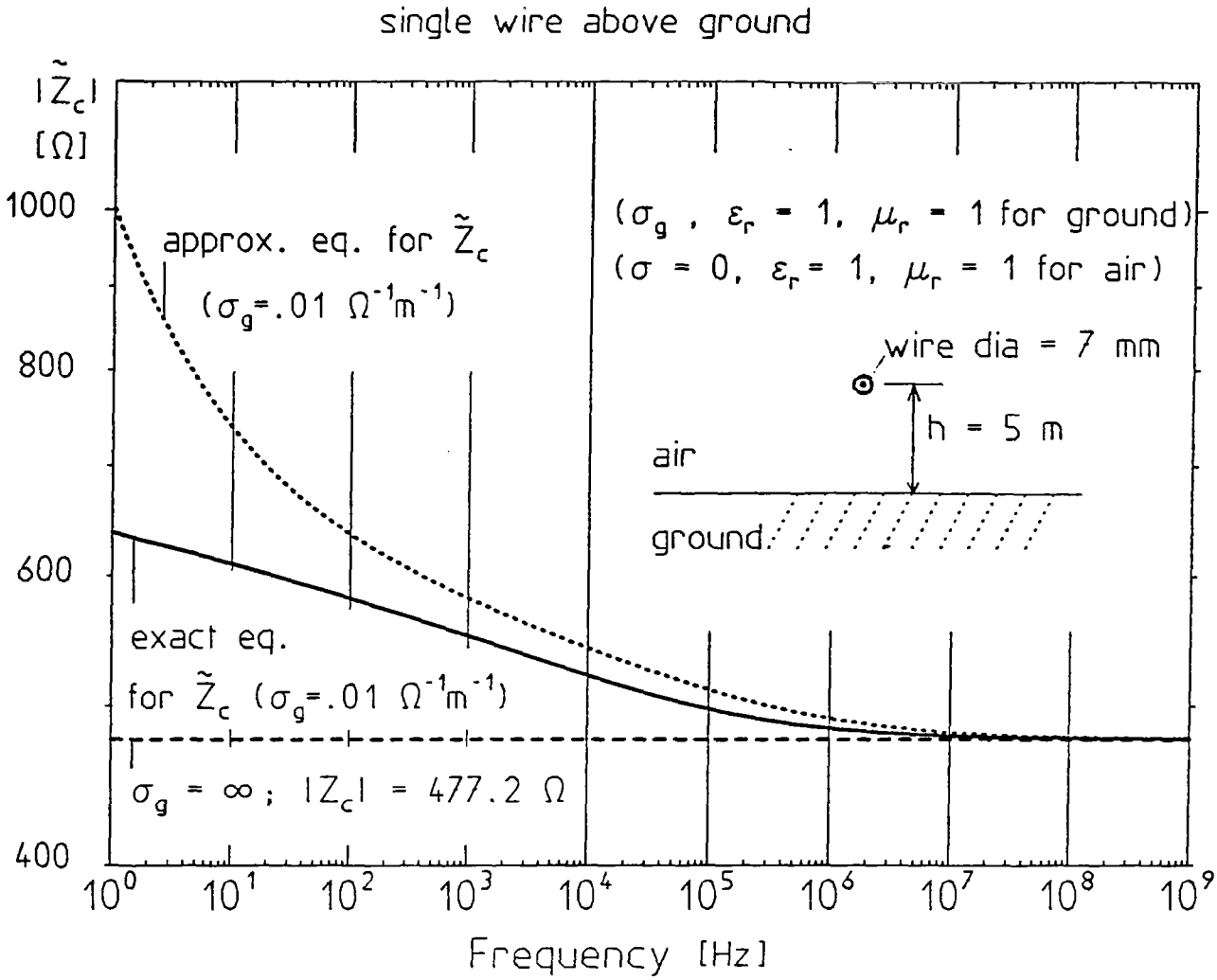

Figure 7. Magnitude spectrum of the characteristic impedance of an aerial wire of dia = 7 mm situated 5 m above ground.

$$\tilde{Q}(x) = \frac{1}{2\,\tilde{Z}_c} \int_{x}^{x_4} e^{-\gamma v}\, \tilde{E}_x(\omega, v)\, dv \qquad (14)$$

and the line extends from $x = x_1$ to $x = x_4$ (as in figure 5). The constants K_1 and K_2 are determined from the terminating impedances Z_1 and Z_2 at $x = x_1$ and $x = x_4$ respectively with $(x_4 > x_1)$. They are given by [1],

$$\tilde{K}_1 = \tilde{\rho}_1\, e^{\gamma x_1} \left[\frac{\tilde{\rho}_2\, \tilde{P}(x_4)\, e^{-\gamma x_4} - \tilde{Q}(x_1)\, e^{\gamma x_4}}{e^{\gamma(x_4 - x_1)} - \tilde{\rho}_1 \tilde{\rho}_2\, e^{-\gamma(x_4 - x_1)}} \right] \qquad (15)$$

$$\tilde{K}_2 = \tilde{\rho}_2\, e^{-\gamma x_4} \left[\frac{\tilde{\rho}_1\, \tilde{Q}(X_1)\, e^{\gamma x_1} - \tilde{P}(x_4)\, e^{-\gamma x_1}}{e^{\gamma(x_4 - x_1)} - \tilde{\rho}_1 \tilde{\rho}_2 e^{-\gamma(x_4 - x_1)}} \right] \qquad (16)$$

in which the reflection coefficients $\tilde{\rho}_1$, $\tilde{\rho}_2$ at the ends of the line are given by

$$\tilde{\rho}_1 = \frac{\tilde{Z}_1 - \tilde{Z}_c}{\tilde{Z}_1 + \tilde{Z}_c} \qquad \tilde{\rho}_2 = \frac{\tilde{Z}_2 - \tilde{Z}_c}{\tilde{Z}_2 + \tilde{Z}_c} \qquad (17)$$

It is observed from the above equations that the line current has resonances at $f_n = n[c/(2\ell)]$ where ℓ is the length of the line (70 m for the present case) under the condition of perfectly conducting ground ($\sigma_g = \infty$) and short or open circuit terminations. This corresponds to about 2.14 MHz of fundamental resonance frequency and harmonics thereof.

The total horizontal field $\tilde{E}_{xv}$ (x, y = h, z = z_1) in the vertical polarization and $\tilde{E}_{xh}$ (x, y = h, z = z_1) in the horizontal polarization are given by [1],

$$\tilde{E}_{xv} = \tilde{E}_{iv}\, e^{-jkx\cos(\psi)\cos(\varphi)}\,(1 - \tilde{R}_v\, e^{-jk2h\sin(\psi)})\,\sin(\psi)\cos(\Phi) \quad (18)$$

$$\tilde{E}_{xh} = \tilde{E}_{ih}\, e^{-jkx\cos(\psi)\cos(\varphi)}\,(1 + \tilde{R}_h\, e^{-jk2h\sin(\psi)})\,\sin(\Phi) \quad (19)$$

with the corresponding incident fields given by [1],

$$\begin{aligned}&\tilde{E}_{iv}\exp\,[-jkx\cos(\psi)\cos(\Phi) + jk\,(y-h)\sin(\psi)]\\ &\tilde{E}_{ih}\exp\,[-jkx\cos(\psi)\cos(\Phi) + jk\,(y-h)\sin(\psi)]\end{aligned} \quad (20)$$

The reflection coefficients for the vertical polarizations are given by

$$R_v = \frac{\varepsilon_r\,(1 + \frac{\sigma_g}{j\omega\varepsilon})\sin(\psi) - [\varepsilon_r\,(1 + \frac{\sigma_g}{j\omega\varepsilon}) - \cos^2(\psi)]^{1/2}}{\varepsilon_r\,(1 + \frac{\sigma_g}{j\omega\varepsilon})\sin(\psi) + [\varepsilon_r\,(1 + \frac{\sigma_g}{j\omega\varepsilon}) - \cos^2(\psi)]^{1/2}} \quad (21)$$

$$R_h = \frac{\sin(\psi) - [\varepsilon_r\,(1 + \frac{\sigma_g}{j\omega\varepsilon}) - \cos^2(\psi)]^{1/2}}{\sin(\psi) + [\varepsilon_r\,(1 + \frac{\sigma_g}{j\omega\varepsilon}) - \cos^2(\psi)]^{1/2}} \quad (22)$$

where ψ is measured form +z in a vertical plane and Φ is measured from -x in a horizontal plane (see figure 5). For the present case of horizontal polarization, the above equations are specialized and even simplify further.

In concluding this section, it is observed that the above equations are useful in computing the Fourier spectrum of the induced current. The inverse Fourier transform was done to get the time behavior of the line currents. The computer routine used for the inverse Fourier transform is not the Fast Fourier Transform (FFT) but a more conventional routine which allows unequally spaced sampling points.

5. Comparison of Theoretical and Experimental Results

The ten experimental configurations investigated in our study have been identified in Table 1 as cases 1 to 10. The measurement of current is performed at two locations x = -35 m and x = -7 m, while the terminations are varied, as listed in Table 1. The results (measured and calculated) are presented in figures 8 to 12. The top portion of these figures contain measured data in time domain and the bottom portion contains the corresponding computed data. Several comments concerning these comparisons are in order.

First of all, it is observed that the comparisons in general are fair and there is a good qualitative agreement and some deviations quantitatively. The dip after the first peak (e.g., cases 1, 3 etc.) needs explanation, as well as the choice of soil conductivity σ_g.

A. Choice of Ground Parameters

With regard to the soil or ground conductivity, it affects:

a) total electric field above the ground, accounting for the ground reflection
b) the characteristic impedance of the transmission line and
c) the propagation factor

To arrive at the choice of σ_g, different values of

$\sigma_g = \infty,\ 10^{-1},\ 10^{-2},\ 10^{-3}\ \Omega^{-1}/m$

were used in a numerical experiment in computing the total horizontal electric field and the induced current in the transmission line for the case 1. These results may be seen in figures 13 and 14, which lead us to use $\sigma_g = 0.01\ \Omega^{-1}/m$. ε_r was also varied as seen in figure 15. The overhead wire response for case 1 is insensitive to ε_r values in the range of 1 to 10.

It is noted that while σ_g is varied, the peak amplitude of the horizonal total electric field is unchanged, but the zero crossing is significantly affected. On the other hand, in the induced current, there is approximately a factor of 2 variation for σ_g changing from ∞ to 10^{-3} and σ_g value of $10^{-2}\ \Omega^{-1}/m$ appears to give the best comparison with experimental results with ε_r of any value between 1 and 10. We have used $\sigma_g = 10^{-2}\Omega^{-1}/m$ and $\varepsilon_r = 1$ for our comparisons and the theoretical calculations will be insignificantly different if we chose $\sigma_g = 10^{-2}\Omega^{-1}/m$ and $\varepsilon_r = 10$.

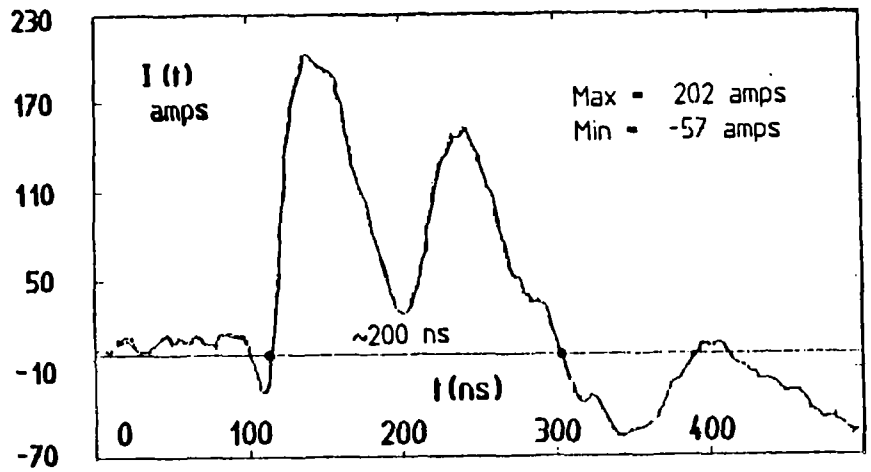

Case 1: Measured at x = -35 m

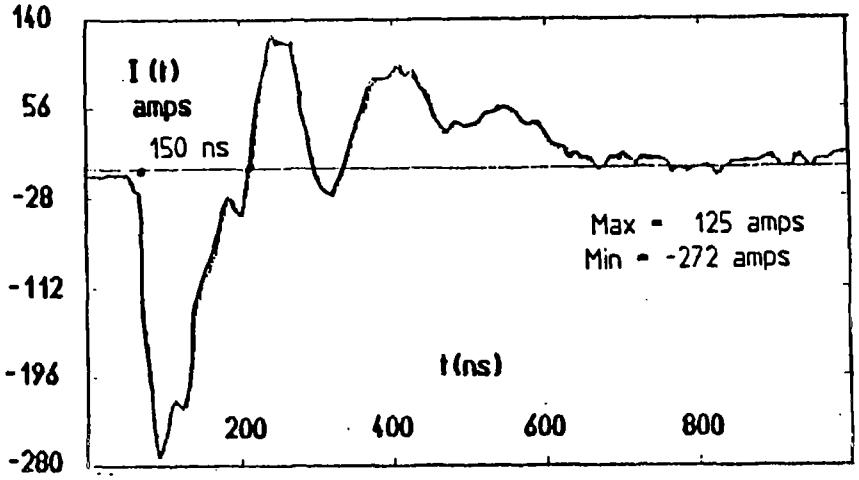

Case 2: Measured at x = -7 m

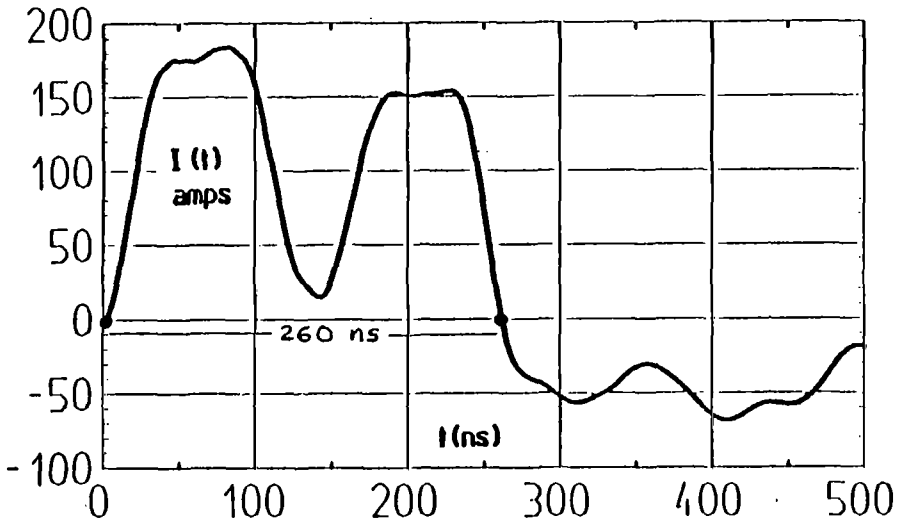

Case 1: Calculated at x = -35 m

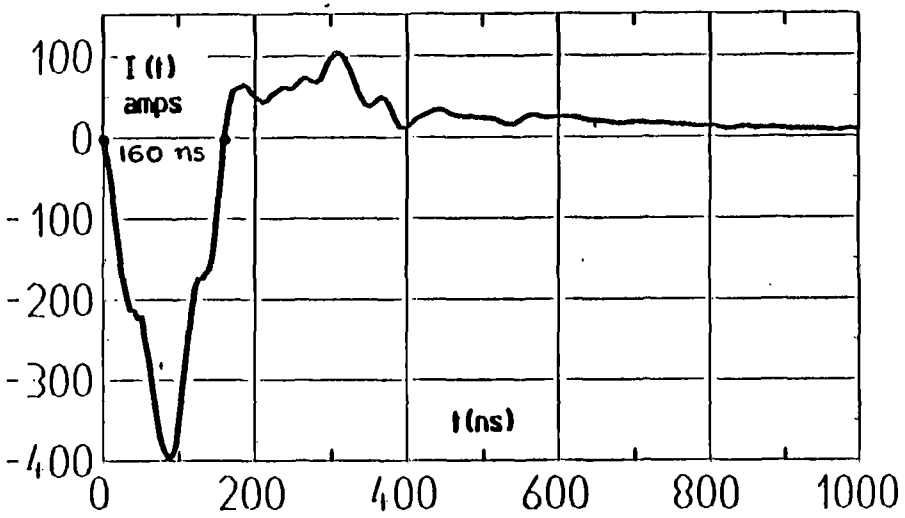

Case 2: Calculated at x = -7 m

Figure 8. Calculated and measured current responses (cases 1 & 2)

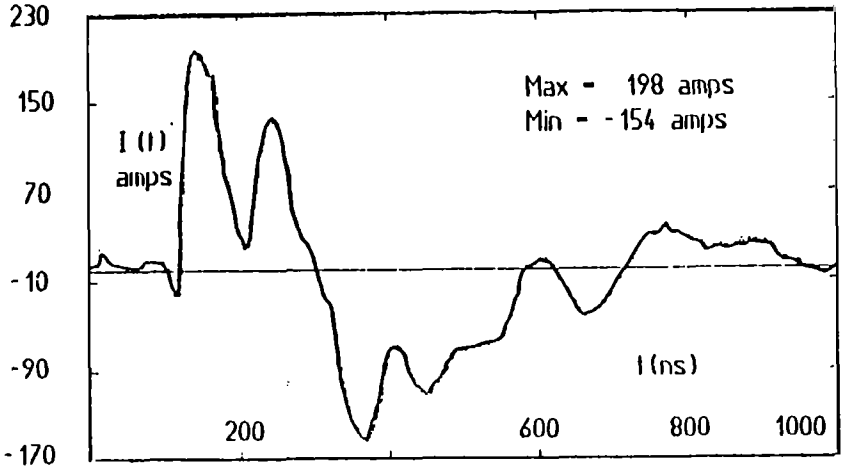

Case 3: Measured at x = -35 m

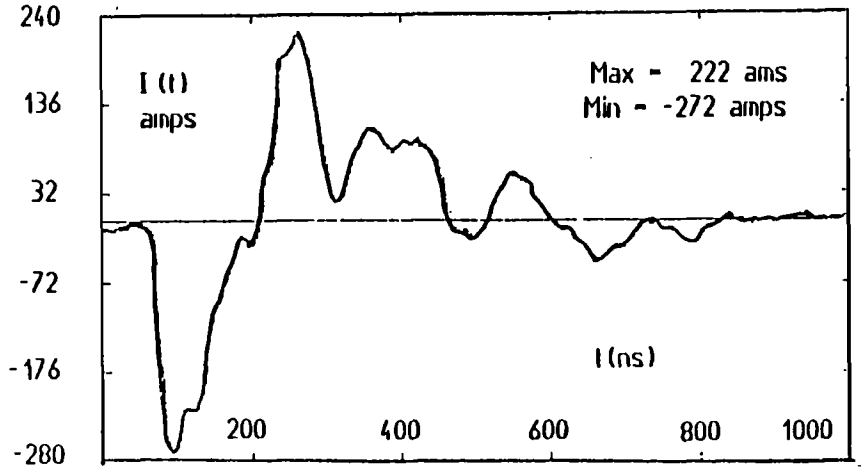

Case 4: Measured at x = -7 m

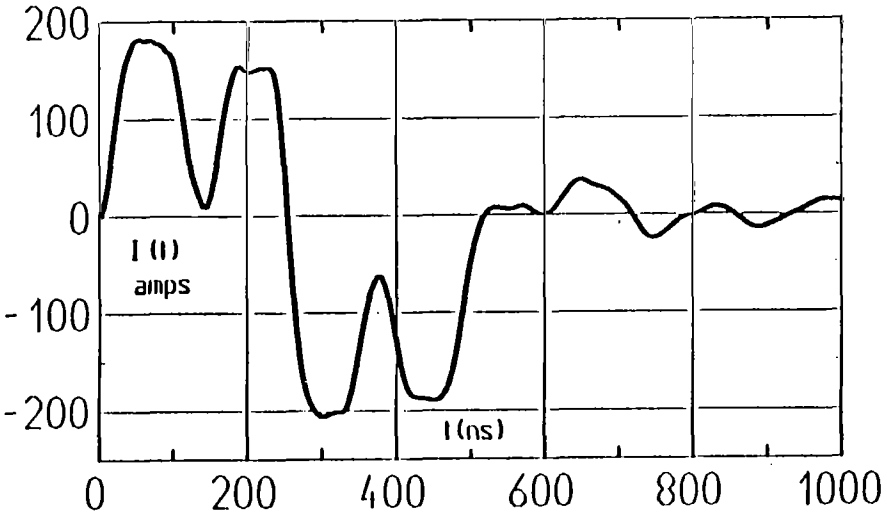

Case 3: Calculated at x = -35 m

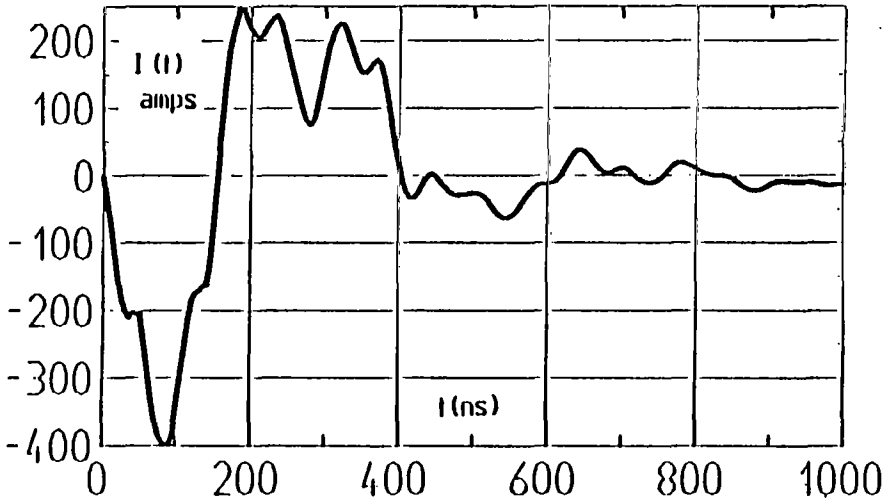

Case 4: Measured at x = -7 m

Figure 9. Calculated and measured current responses (cases 3 and 4)

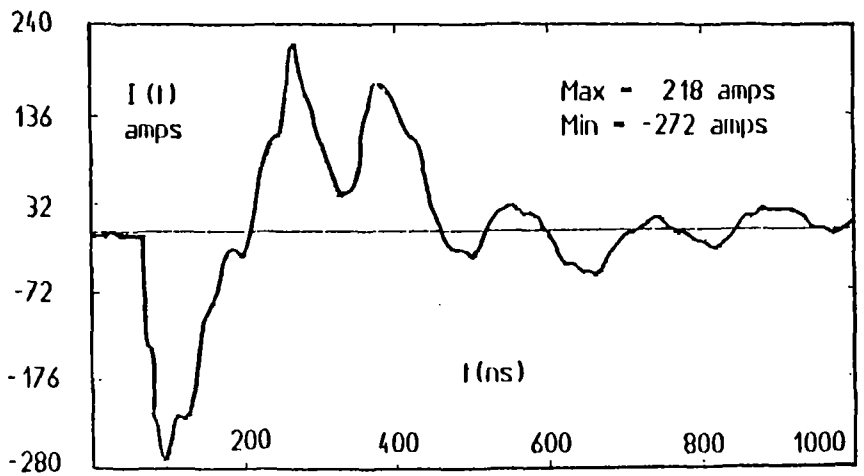

Case 5: Measured at x = -7 m

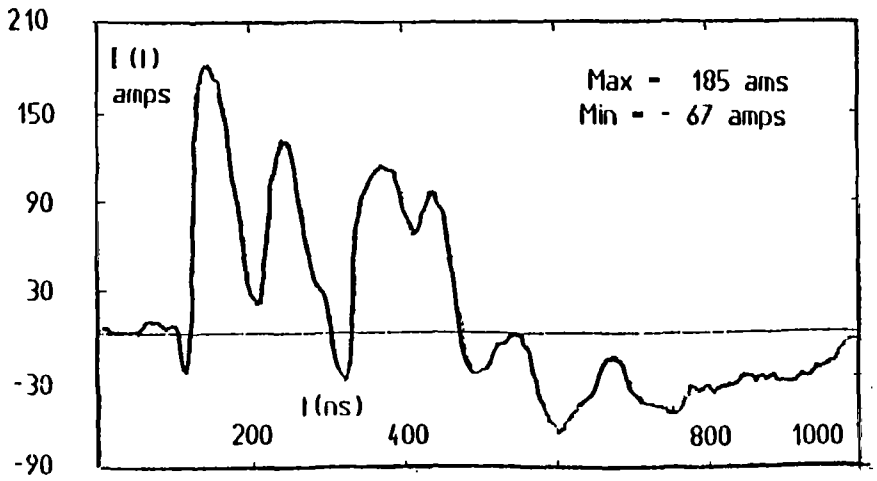

Case 6: Measured at x = -7 m

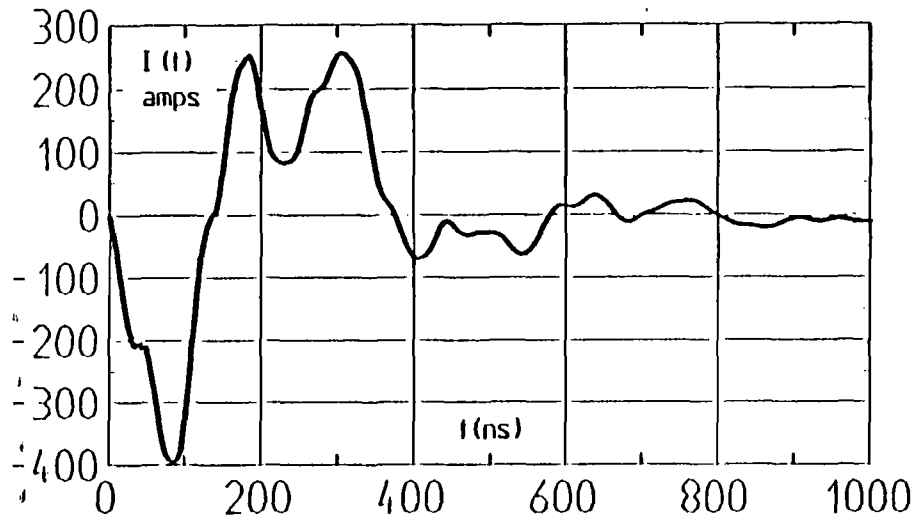

Case 5: Calculated at x = -7 m

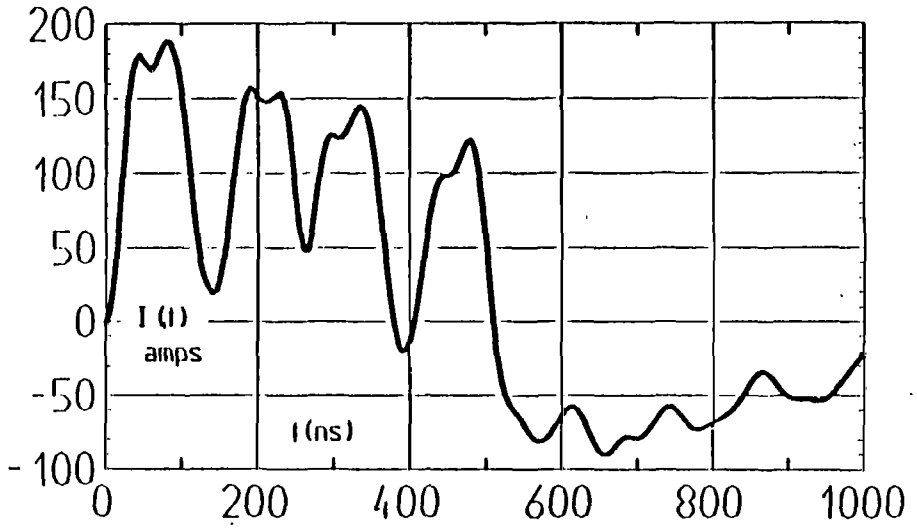

Case 6: Measured at x = -7 m

Figure 10. Calculated and measured current responses (cases 5 and 6)

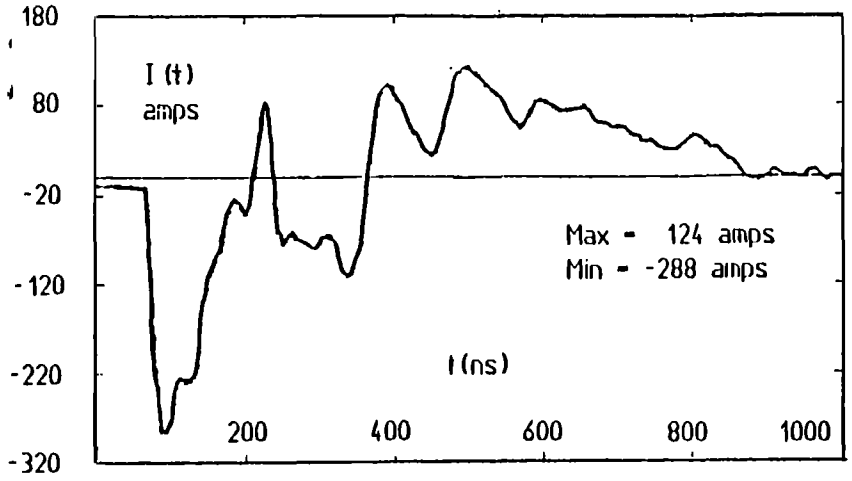

Case 7: Measured at x = -7 m

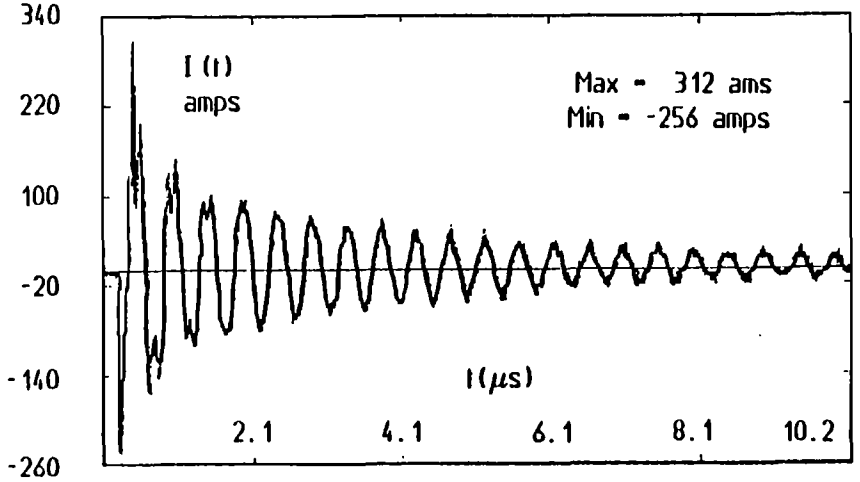

Case 8: Measured at x = -7 m

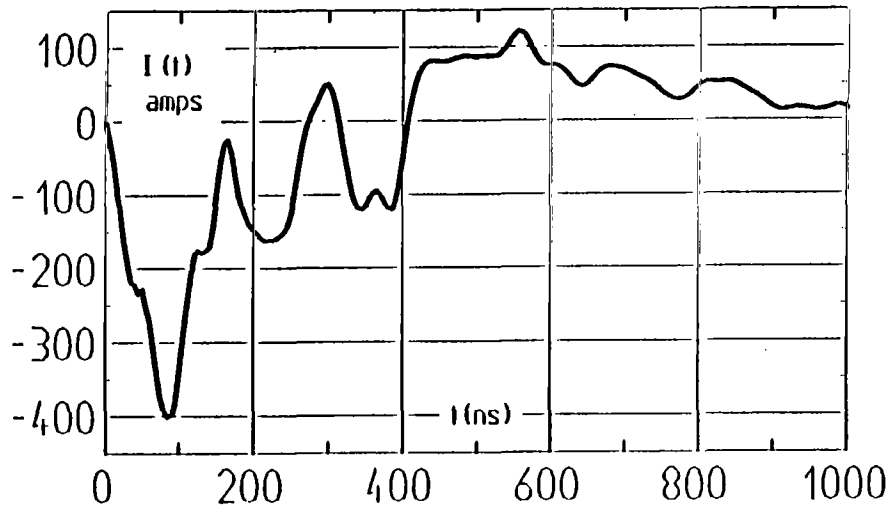

Case 7: Calculated at x = -7 m

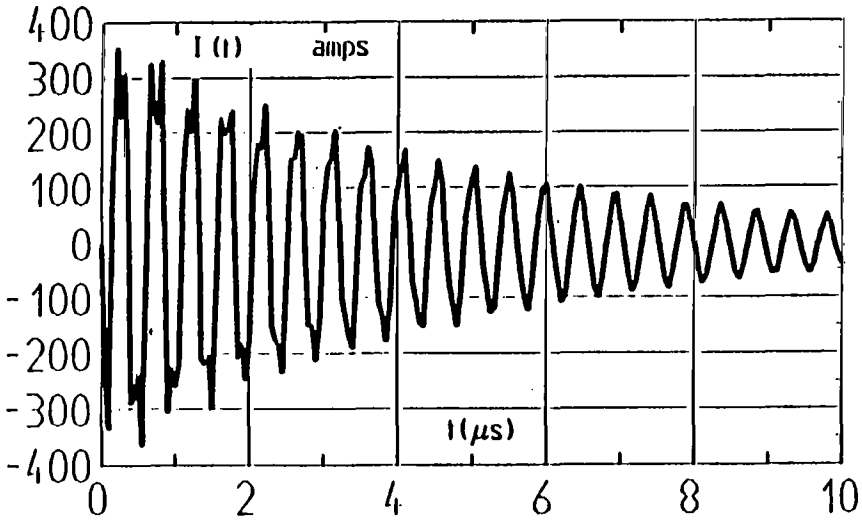

Case 8: Measured at x = -7 m

Figure 11. Calculated and measured current responses (cases 7 and 8)

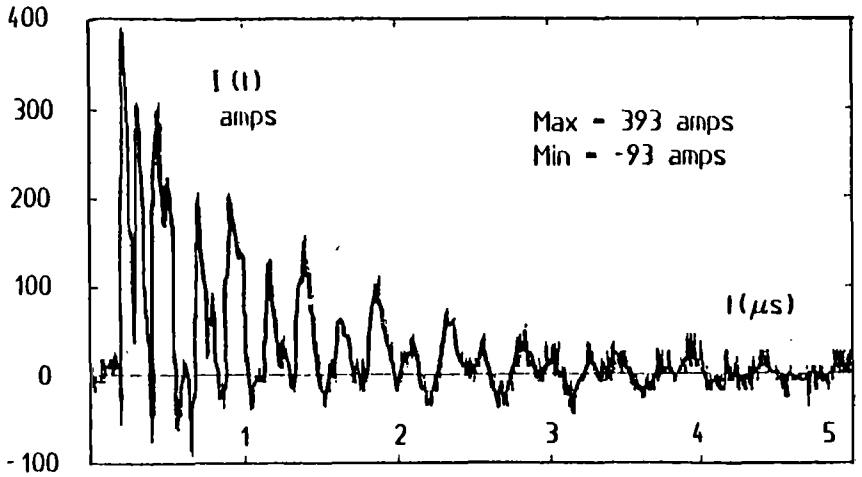

Case 9: Measured at x = -35 m

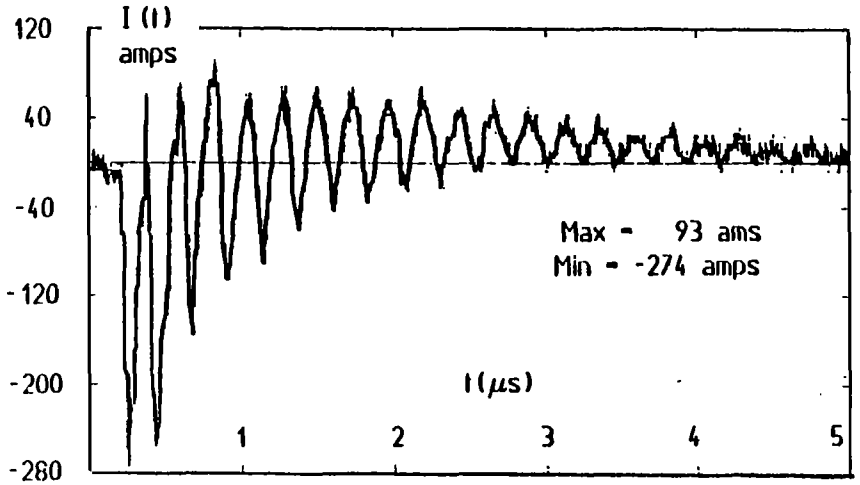

Case 10: Measured at x = -7 m

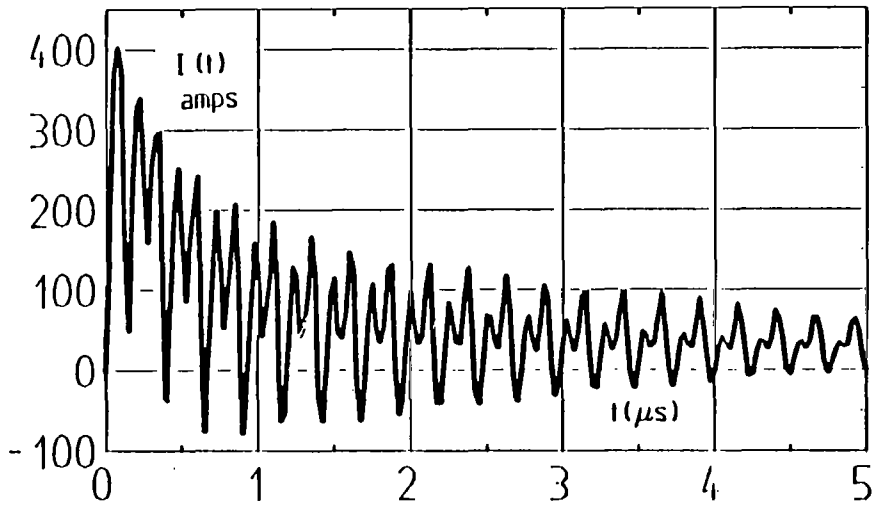

Case 9: Calculated at x = -35 m

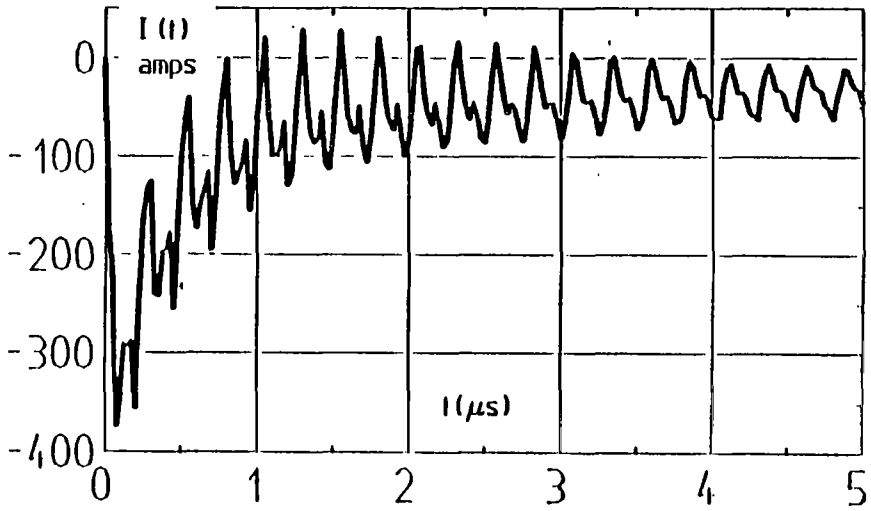

Case 10: Measured at x = -7 m

Figure 12. Calculated and measured current responses (cases 9 and 10)

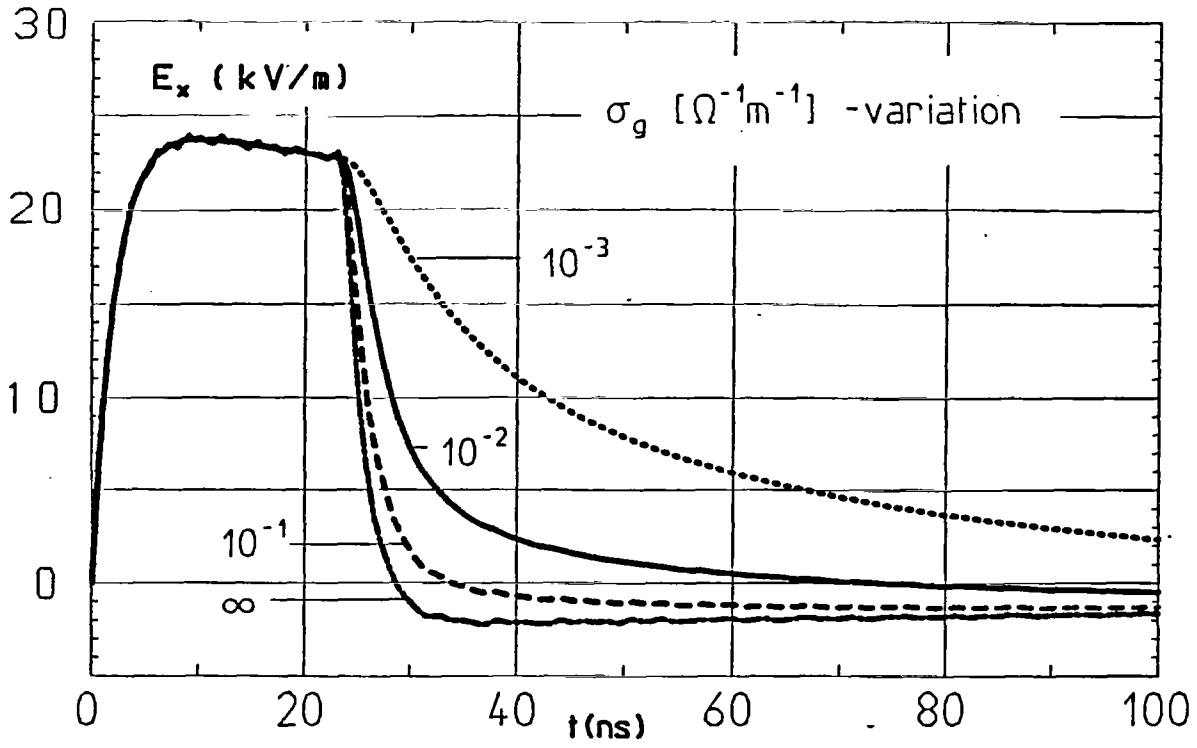

Figure 13. Horizontal electric field after ground reflection at a height of 5 m above ground with varying σ_g

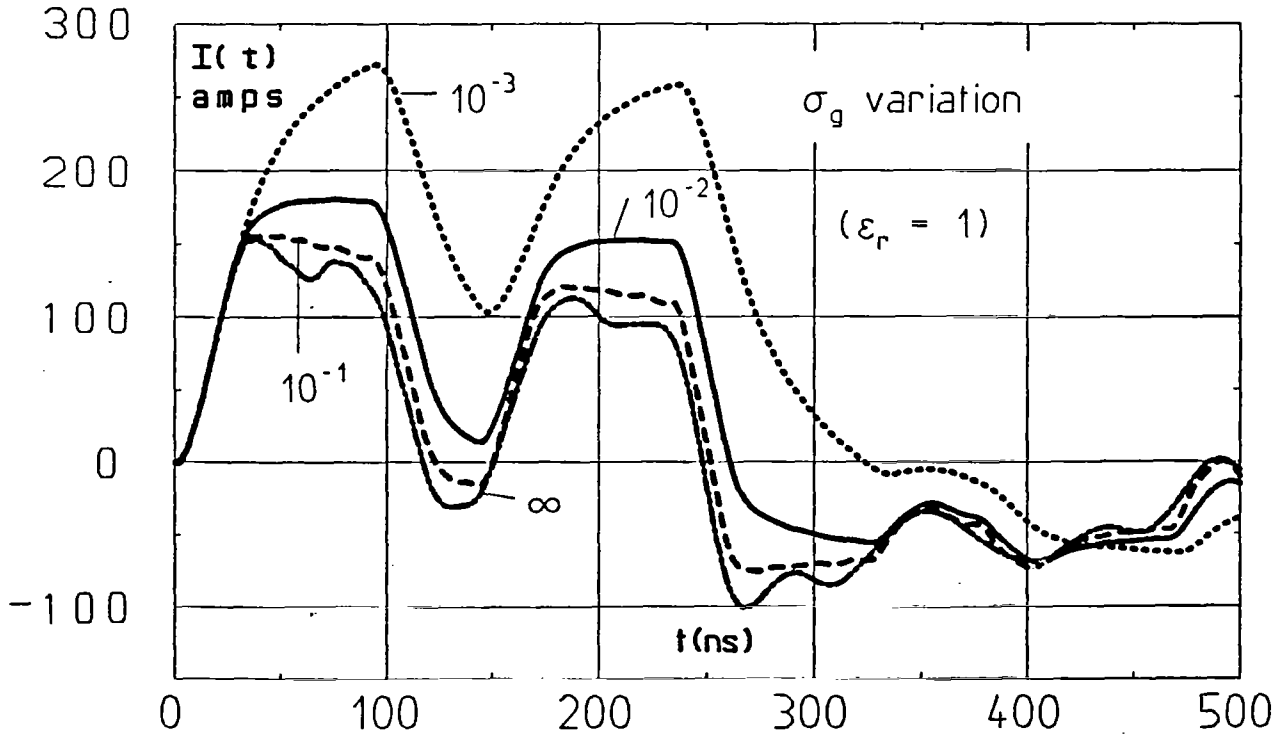

Figure 14. Induced current (computed) for Case 1, with varying σ_g

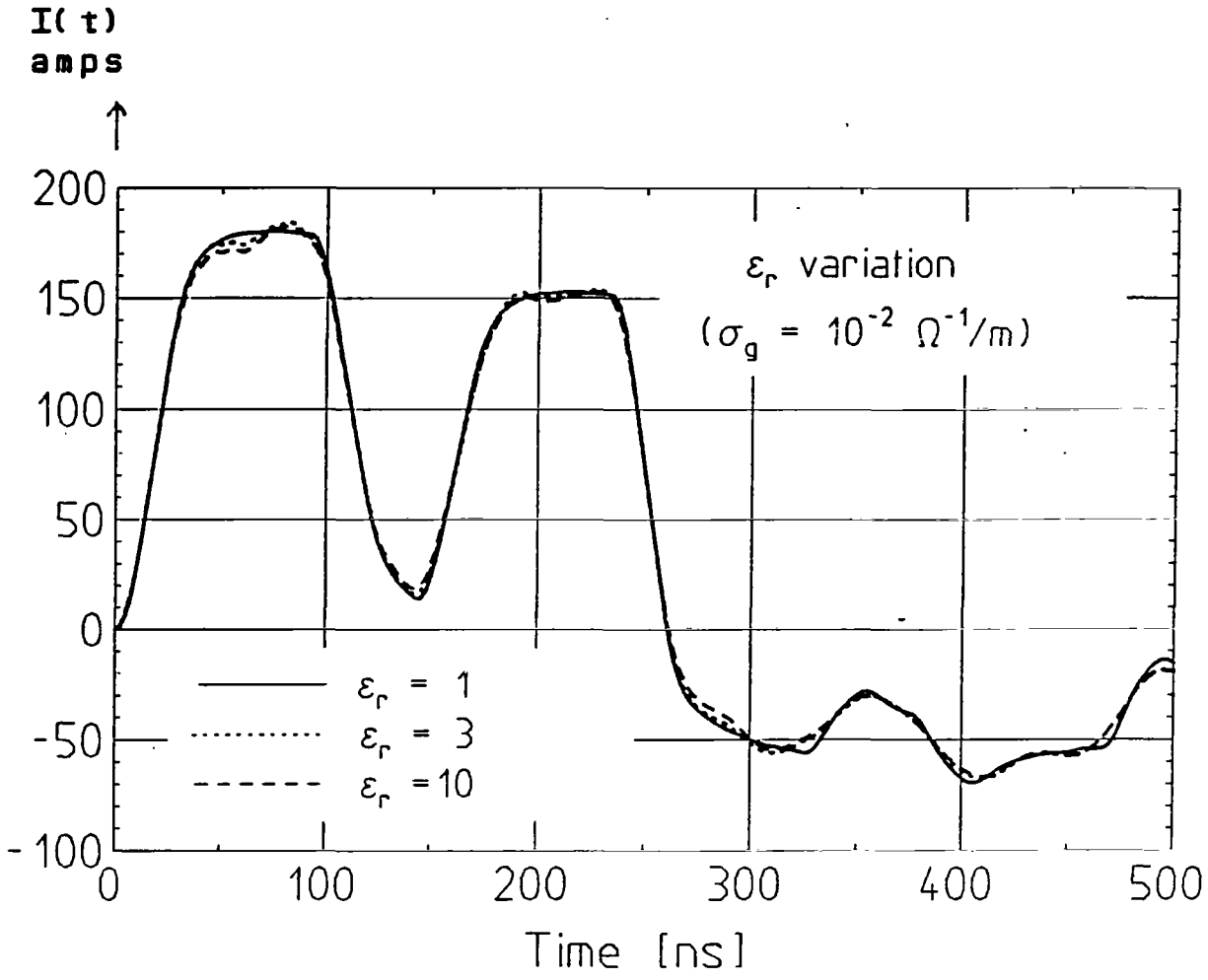

Figure 15. Induced current (computed) for Case 1 with varying ε_r for σ_g = 10^{-2} Ω^{-1}/m.

Note: The induced current is insensitive for ε_r variation between 1 and 10.

B. Local Field Variations

The subject of localized electric field variation due to the presence of the locomotive has been discussed earlier (see figure 5) in equation (3) where a position dependent constant was introduced. The constant f_2 in section 2 of figure 5 was varied in a set of numerical experiments shown in figure 16. Once again, the conclusion was that $f_2 = 0.1$ leads us to the best comparison with experimental results.

C. Temporal Behavior of the Incident Field

As was mentioned at the end of section 2, the transmission line current reponses have been computed using a double exponential NEMP incident field of the form

$$E_o \, (e^{-\alpha t} - e^{-\beta t}) u(t)$$

with

$\alpha = 4 \times 10^6/s$

$\beta = 4.8 \times 10^8/s$

However, it is well known that the MEMPS like facility cannot generate exactly a double exponential type of field. So the question arises whether a moderate variation in α and β can lead to small or large variations in the transmission line currents. α was varied in steps from $2 \times 10^6/s$, $4 \times 10^6/s$ and $8 \times 10^6/s$, keeping β fixed at $4.8 \times 10^8/s$. For these 3 cases, the total horizontal electric field (incident double exponential + ground reflections) and the induced current in the transmission line are computed. These are shown in the top half of figure 17. Next, we studied the impact of changing β values from $1 \times 10^8/s$, $4.8 \times 10^8/s$ and $1 \times 10^9/s$, keeping α fixed at $4 \times 10^6/s$. Similar calculations of the total field and induced

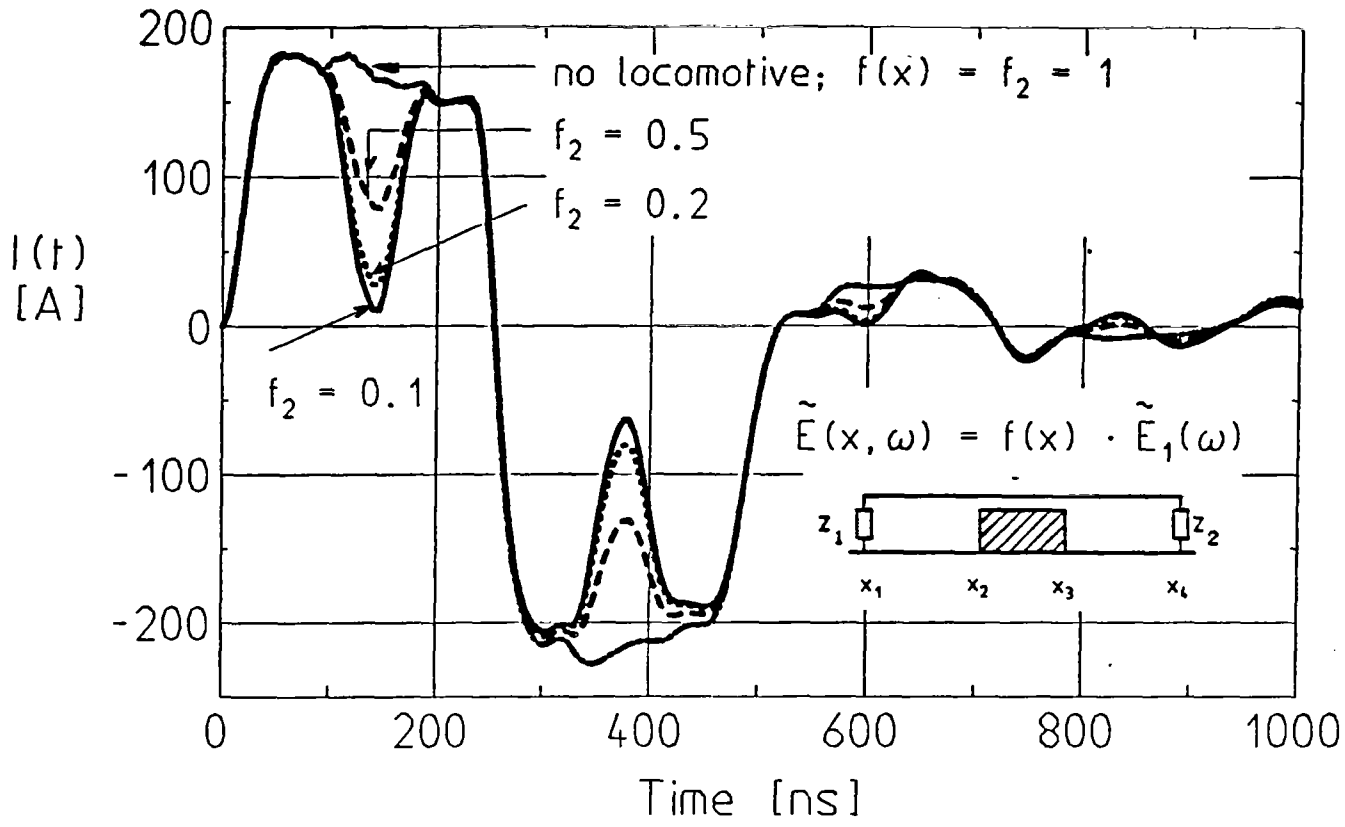

Figure 16. Induced current I (t) in amps, computed for the case 3 (Table 1), with varying value of f_2 (equation 3).

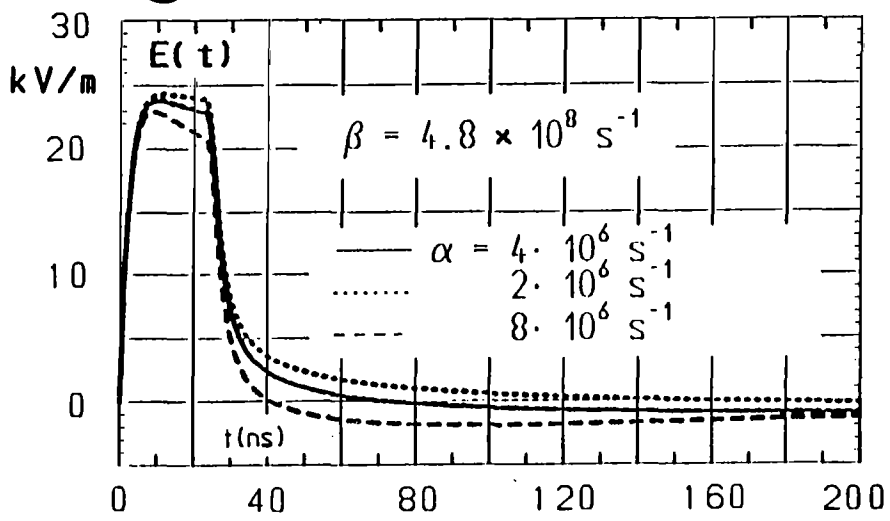

a) Double exponential E field $E_0(e^{-\alpha t} - e^{-\beta t})\ u(t)$ after reflection at ground ($\sigma_g = 10^{-2}\ \Omega^{-1}/m$, $\varepsilon_r = 1 \ldots 10$) for various values of α at h=5 m above ground.

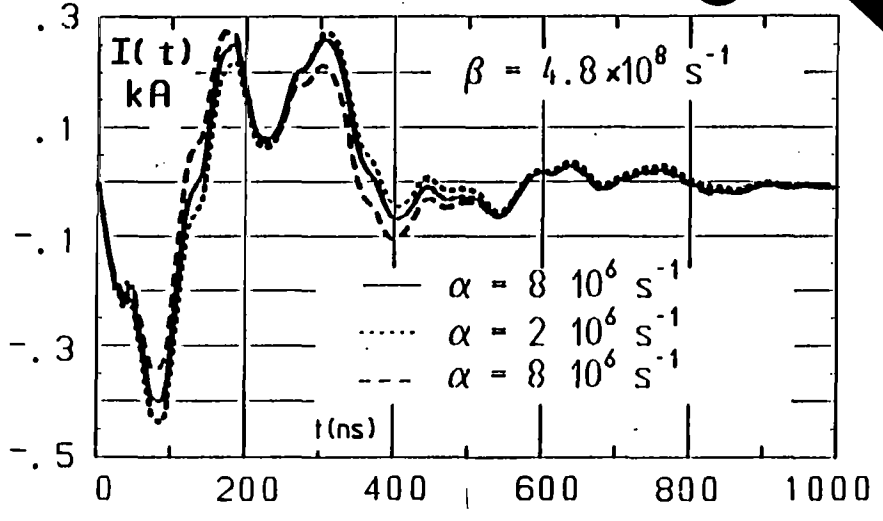

b) Induced current in transmission line corresponding to α values in (a) Case 5 of figure 11, for comparison

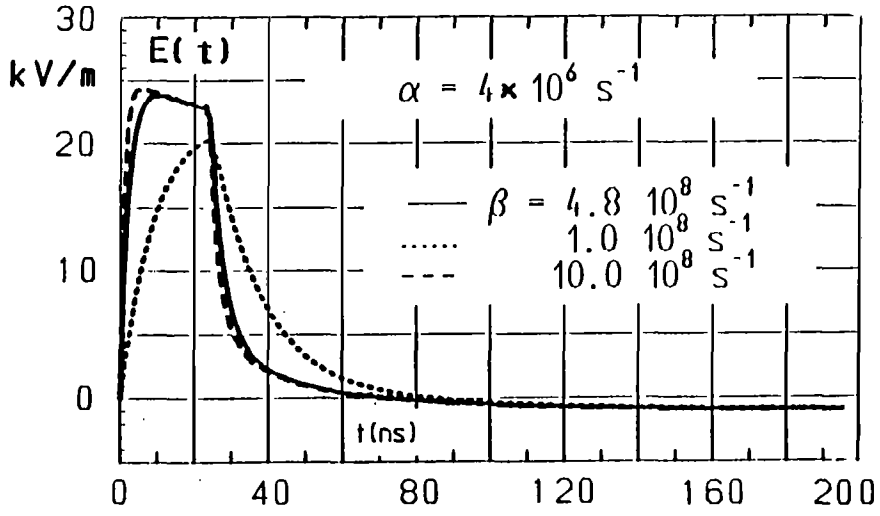

c) Double exponential E field $E_0(e^{-\alpha t} - e^{-\beta t})\ u(t)$ after reflection at ground ($\sigma_g = 10^{-2}\ \Omega^{-1}/m$, $\varepsilon_r = 1 \ldots 10$) for various values of β at h=5 m above ground.

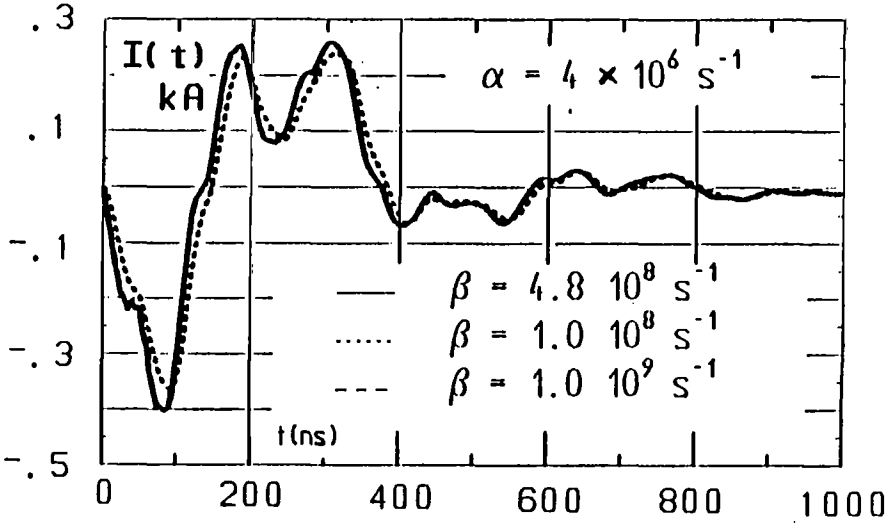

d) Induced current in transmission line corresponding to β values in (c) Case 5 of figure 11, for comparison

Figure 17. Numerical experiments for studying the effects of α and β.

current were performed and the results are shown in the bottom part of figure 17. The ground characteristics ($\epsilon_r = 1$ and $\sigma_g = 10^{-2}\ \Omega^{-1}/m$) are held fixed during these computations.

From the above numerical experiments, it is observed that the electric field component parallel to the transmission line is not significantly affected by a moderate variation in α and β, due to the superposition of the incident and ground reflected waves. The rise parameter β has more influence on the electric field than the decay parameter α . The induced current on the transmission line is somewhat independent of the detailed field shape because the time constant of the response is quite large compared with that of the field.

D. The Current Return Path

The wire above ground forms a transmission line, typically with the imperfectly conducting ground medium as the return conductor. However, in the present situation, we have the terminating impedances connected to the rails rather than the ground. This strictly means, the return current is shared by the rails and the soil medium. The rails are electrically, however weakly, connected to the ground medium. So, the question arises whether one has a two-wire line with the return conductor placed at the interface of air and soil media ? Or do we have an aerial wire above ground ? The answer of course is frequency dependent, as may be seen in figure 7. At low frequencies, the wave impedance is dependent strongly on σ_g, but at frequencies > 1 MHz, the wave impedance approaches asymptotically the $\sigma_g = \infty$ value. The exact nature of rail coupling to the ground has not been studied and hence the division of the return current into rail current and soil current is unknown, in terms of its frequency dependence.The approximation of the aerial wire above ground, as opposed to a two wire line with the rails as a return conductor can only be justified over the high frequency portions.

Finally, with reference to cases 1 and 2 contained in figure 8, the following observations can be made.

Time interval to first zero crosssing is 200 ns (measured) and 260 ns (calculated) and the peak currents are 202 amps (measured) and 177 amps (calcualted), for case 1. For case 2, the time interval to first zero crossing is 150 ns (measured) and 160 ns (calculated) and the peak currents are -272 amps (measured) and -375 amps (calculated). Considering all of the approximations that had to be made in arriving at the computed results, such deviations are not difficult to understand and perhaps improved modelling of the incident field will result in better computations.

It is noted that in all of the theoretical and experimental comparisons shown in figures 8 to 12, the computed results have the following approximations built in.

1. The incident field is modelled by a double exponential and the sensitivity to its shape parameters has been studied.

2. The total horizontal field is estimated as a combination of the incident and ground reflected waves.

3. The ground medium is characterized by $\varepsilon_r = 1$ (overhead wire responses are insensitive for a range of ε_r values from 1 to 10) and $\sigma_g = 10^{-2}\ \Omega^{-1}/m$, leading to the best possible comparison between the theory and experiment.

4. The presence of the locomotive at the center of the transmission line is accounted by modifying with a constant multiplier, the uniform field observed in the incident electromagnetic wave. Such a modification leads us to understand and interpret the wave shape of the current responses in the transmission line.

5. The vertical electric field parallel to the terminating impedances are neglected in the present study.

6. Concluding Remarks

We have adressed the problem of investigating the current responses on a wire above ground situated near a hybrid type of NEMP simulator. The simulator facility is the MEMPS in Switzerland. Theoretical approaches are available in the literature for computing the transmission line responses. However, certain extraneous features were present during the experiment e.g., the presence of a locomotive over a small portion of the overhead wire and the necessary rails, which affects the return path. In effect, the theoretical analysis is for somewhat idealized situation and the actual experiment was with engineering compromises present. The presence of the locomotive has a significant effect and can be empirically acounted for by modifying the incident fields over a portion of the wire.

It was also observed that the MEMPS facility generates a horizontal field parallel to the wire which is fairly uniform over the entire 70 m length of the wire, in the absence of the wire and the locomotive. The wire responses have been studied with varying termination impedances. It is well known and observed here, that the line resonances are seen if the terminations differ considerably (short or open circuit nominally) from the characteristic impedance of the wave propagation along the line.

A set of numerical experiments were performed as a part of sensitivity analysis to determine the effect of soil conductivity, local field strength variations, temporal shape of the incident field prior to combining with the ground reflections etc. The agreement between the computations and experimental results are seen to be fair both in a qualitative and quantitative sense.

References

1. E.F. Vance, Coupling to Shielded Cables, John Wiley and Sons, 1987

2. A.A. Smith, Coupling of External Electromagnetic Fields to Transmission Lines, John Wiley and Sons, 1977

3. M. Aguet, M. Ianos and C.-C. Lin, "Transient Electromagnetic Field Coupling to Long Shielded Cables", IEEE Transactions on EMC, Vol. EMC-22, No. 4, pp 276-282, November 1980

4. E.D. Sunde, Earth Conduction Effects in Transmission Systems, Van Nostrand, New York 1949

5. S. Ramo, J.R. Whinnery and T. Van Duzer, Fields and Waves in Communication Electronics, John Wiley and Sons, 1984 edition, Chapter V, pp 210-225

6. J.C. Giles, "A Survey of Simulators of EMP Outside the Source Region, Some Characteristics and Limitations", Presented at NEM 1984, Baltimore, Maryland, July 1984

7. H.D. Bruens, "Pulserregte elektromagnetische Vorgaenge in dreidimensionalen Stabstrukturen", University of the German Federal Armed Forces, Hamburg, Germany, Thesis 1985